

I.A. VESELOVSKI^{1,✉}
H.K. CHA²
D.H. KIM²
S.C. CHOI²
J.M. LEE²

Study of atmospheric water in gaseous and liquid state by using combined elastic–Raman depolarization lidar

¹ Physics Instrumentation Center of General Physics Institute, Troitsk, Moscow 142 190, Russia

² Korean Atomic Energy Research Institute, P.O. Box 105, Yusong, Taejon 305-600, Korea

Received: 12 December 2000/

Revised version: 27 September 2001

Published online: 7 November 2001 • © Springer-Verlag 2001

ABSTRACT A combined elastic–Raman lidar system based on a tripled Nd:YAG laser is used for the separate detection of elastic backscatter and Raman signals from atmospheric nitrogen, water vapor and liquid water and for their depolarization measurement. Vertical profiles of water-vapor and liquid-water content measured under clear-sky conditions behave differently: inside the boundary layer the ratio of liquid-water to water-vapor Raman backscatters rises with altitude. The depolarization measurements bring additional information about atmospheric scattering. The observed depolarization ratio of the water-vapor Raman signal is about 14%, while for liquid water this ratio varies in the 30%–75% range, which exceeds the depolarization of bulk water and is attributed to the water-aerosol effects. Raman contours of water vapor and liquid water are partially overlapped, and bleed-through of liquid-water Raman backscatter leads to enhancement of depolarization of the water-vapor Raman signal. This parameter may be used as a convenient indicator of liquid-water interference in water-vapor measurements.

PACS 42.62.Fi, 42.68.Ge, 42.68.Jg, 42.68.Mj, 42.68.Wt

1 Introduction

The application of the lidar technique to gain more information about the planetary boundary layer (PBL) is a ripe research area. Combined elastic–Raman systems are commonly used for the evaluation of aerosol backscattering – extinction characteristics and water-vapor content [1–4]. Several attempts to extend the Raman technique to include liquid-water scattering were made recently [5–7]. Water in the PBL exists in the form of water droplets or water-laden aerosols. Knowledge of the aerosol parameters and integral water content is essential in the physics of clouds, and in the study of atmospheric photochemistry and electricity. In our previous paper we reported the separate detection of water-vapor and liquid-water Raman backscatters [7]. In the present study we

complement this method by measuring depolarization of the elastic and Raman signals.

The depolarization technique is traditionally applied to elastic backscatters for discrimination of solid- and liquid-phase clouds and aerosols [8–11]. To our knowledge the only attempt to use the depolarization of the nitrogen Raman signal for discrimination of multiple scattering by irregular particles was made by Wandinger et al. [12]. At the same time, the depolarization of liquid-water and water-vapor Raman signals also contains useful information about atmospheric scattering. In contrast to Mie backscattering, which does not change the polarization state, the incoherent Raman scattering in liquid droplets introduces polarization changes [13]. The value of the depolarization depends on the refraction coefficient and on droplet size, so that the altitude profiles of the depolarization ratio may contain information about the aerosol. The depolarization of Raman backscatter from water droplets is higher than that of water vapor, and bleed-through of liquid-water scattering in the vapor channel should lead to increases in the depolarization of the water-vapor Raman signal. Hence, the depolarization may serve as an indicator of liquid-water interference in water-vapor measurements. This problem is especially severe when wide-band excimer lasers are used [5].

2 Lidar-system description

2.1 Raman signals of water vapor and liquid water

The large energy distribution of the liquid-water Raman-backscattering contour allows us to select a spectral region where it does not overlap the water-vapor Raman line. Figure 1 illustrates the choice of operational wavelengths. The Raman spectrum of liquid water in backscattering geometry, measured by Whiteman et al. [14] at 23 °C, is shown together with spectral transmittances of the filters used for selection. The filter for liquid water is centered at 401.5 nm; its transmittance is 12% at maximum and 0.15% at 407.8 nm (water-vapor line). The effects related to temperature dependence of the water Raman contour may be diminished by using a narrow-band (< 0.5-nm) filter centered near the isosbestic point at 403.7 nm [14], but it significantly decreases the water Raman backscatter. So in the present study we have not taken the errors related to temperature variations into consideration.

✉ Present address: NASA Goddard Space Flight Center, Code 924, Greenbelt, MD 20771-0001, USA.
E-mail: iveselov@pop900.gsfc.nasa.gov

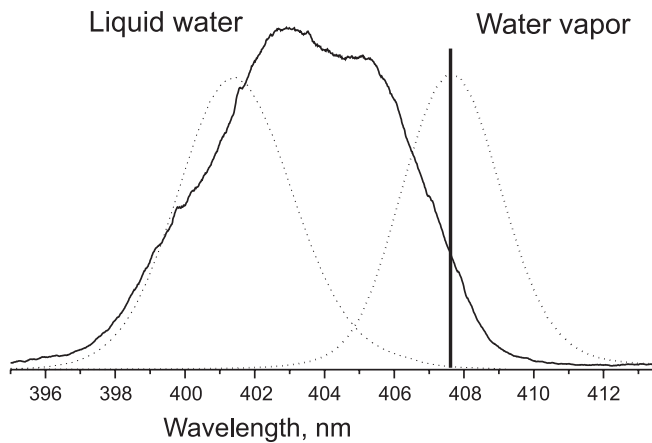


FIGURE 1 The Raman spectrum of liquid water at 23 °C measured by Whiteman et al. [14]. The *dashed line* shows the spectral transmittances of the interference filters used for the spectral selection of liquid-water and water-vapor Raman signals. The *vertical solid line* indicates the position of the water-vapor Raman line

The water-vapor content is usually calculated from the ratio of vapor (P_{vap}) and nitrogen (P_{nitr}) Raman signals [1]:

$$C_{\text{vap}} = K \frac{P_{\text{vap}}(z)}{P_{\text{nitr}}(z)} \times \frac{\sigma_{\text{nitr}}}{\sigma_{\text{vap}}} \times \frac{\exp \left[- \int_{z_0}^z (\alpha_{\text{nitr}}^A(\xi) + \alpha_{\text{nitr}}^M(\xi)) d\xi \right]}{\exp \left[- \int_{z_0}^z (\alpha_{\text{vap}}^A(\xi) + \alpha_{\text{vap}}^M(\xi)) d\xi \right]}$$

where $\sigma_{\text{nitr,vap}}$ are the Raman-backscattering cross sections and $\alpha_{\text{nitr,vap}}^{A,M}$ are the aerosol and molecule extinction coefficients for the nitrogen and water-vapor Raman signals. The calibration parameter K is determined from the transmittance of optical elements and from the ratio of photomultipliers' (PMTs') sensitivities. The measurements were performed only for clear-sky conditions and the maximal sounding altitude usually did not exceed 2 km, so that the errors related to differential molecular and aerosol extinction are small. For example, even for an average aerosol extinction of 0.5 km^{-1} the corresponding error is about 5%. Aerosol-extinction correction in our data processing is ignored, although the molecular one is included.

The estimation of the Raman-scattering cross section for liquid droplets is very complicated. The factors contributing to the backscattering are considered in [5, 7]. An accurate and quantitative evaluation of liquid-water content from the Raman measurements probably cannot be performed without calibration measurements in the aerosol chamber. Thus, at present, we can talk only about the relative behavior of water-vapor and liquid-water Raman signals.

2.2 Depolarization of Raman signals

If a receiver selects parallel P_{\parallel} and cross-polarized P_{\perp} backscattering powers, the depolarization ratio of the scattered signal is calculated as $\delta = P_{\perp}/P_{\parallel}$. For the vibrational Raman scattering in gases this ratio depends on molecular parameters and on contributions from the nearest Raman rotational spectrum. The depolarization ratio for the Q-branch of water vapor is $\delta_{\text{v}} < 6\%$ [15]. The value of δ_{v} measured in our

lidar system should be higher because of the contribution from rotational wings. Depolarization of liquid water δ_{liq} is the sum of the bulk water depolarization δ_{liqB} and the depolarization introduced by water droplets δ_{liqDr} :

$$\delta_{\text{liq}} = \delta_{\text{liqB}} + \delta_{\text{liqDr}}.$$

The depolarization ratio of bulk water δ_{liqB} depends on vibrational frequency; in our operational spectral region, at $T = 21 \text{ }^{\circ}\text{C}$, δ_{liqB} is around 15% [16]. It should be noted that the water Raman contour in the spectral interval 405–410 nm, where it overlaps the transmittance band of the water-vapor channel, is characterized by a higher depolarization ratio, up to 30%.

The value of δ_{liqDr} depends on a complex refractive index n and on droplet size; hence it is range-dependent. Model calculations of δ_{liqDr} for the scattering of dipoles embedded in spheres were performed by Kerker and Druger [13]. These calculations in backscattering geometry were done only for several values of the size parameter and for refractive indices $n = 1.1$ and 1.5 . In general the depolarization grows with size-parameter increase. For the estimation of depolarization introduced by Raman scattering in droplets an accurate computer simulation is needed. Development of such a computer code is in progress. At present we focus at the experimental determination of values of liquid-water Raman-signal depolarization and the range of its variation.

2.3 Experimental setup

The radiation source in our lidar system is a tripled Nd:YAG laser of 120-mJ energy and 30-Hz repetition rate. The backscattered signal is collected by a 30-cm-aperture Newtonian telescope; in the two-channel spectrum analyzer the Glan prism separates the optical signals with polarizations parallel and perpendicular to the initial one. In our experiments we measured elastic backscattering and Raman signals from nitrogen Raman (386.7 nm), liquid water (401.5 nm) and water vapor (407.8 nm). The change of operational wavelengths is achieved by replacement of interference filters. The signals are detected by PMTs operated in analog mode. For suppression of elastic backscatter, the interference filters are combined with dichroic mirrors. The details of system design together with filter parameters are presented in [7].

The measurements were performed at night, during October to November 1999, in Taejon, South Korea. In one typical Raman profile 10 000 laser pulses are accumulated and the profiles smoothed with a 100-m averaging interval. In our two-channel system we are unable to detect all the backscattered components of interest simultaneously. Thus, a delay between every profile, about 10 min, is introduced. The measurements were made only under clear-sky conditions. To exclude the effects related to abrupt atmospheric changes, the series of measurements were repeated. The results of depolarization measurements are corrected for the difference in the sensitivity of the channels and cross-talk effects. After correction, the depolarization of the elastic signal in the aerosol-free region is about $1.5 \pm 0.2\%$, typical for atmospheric molecule depolarization [11].

3 Results

For the evaluation of aerosol-extinction coefficients both Klett [17] and Raman [1,2] methods are used. These methods yield similar results when the variations of the lidar ratio inside the PBL are small. The extinction profiles are calculated for altitudes above 600 m, where the geometrical factor is close to unity. We present the results of liquid-water and water-vapor Raman measurements as the ratios of parallel-polarization components of these signals to the corresponding component of nitrogen Raman backscatter ($P_{\text{vap}}/P_{\text{nitr}}$ and $P_{\text{liq}}/P_{\text{nitr}}$). The Raman signals are corrected for the optical filters' transmittance. As a result the ratio $P_{\text{vap}}/P_{\text{nitr}} = 0.1$ corresponds to a vapor mixing ratio of 20 ± 2 g/kg.

Figure 2 presents the ratios $P_{\text{vap}}/P_{\text{nitr}}$ and $P_{\text{liq}}/P_{\text{nitr}}$ of the aerosol-extinction profile evaluated by the Klett method and depolarization ratios of elastic and Raman signals obtained on 29 October 1999. During our experiments the only information about temperature and relative humidity at 27-m height was supplied by the Environmental Engineering Group of KAERI. For the profiles presented in Fig. 2, these are 7 °C and 63% and the corresponding water-vapor mixing ratio is 6 g/kg. The water-vapor mixing ratio calculated from li-

dar measurements at 400-m height is about 4.8 g/kg. The water-vapor mixing ratio sharply decreases above the PBL top, while the $P_{\text{liq}}/P_{\text{nitr}}$ ratio does not vary significantly up to 1500-m altitude.

The nitrogen Raman signal depolarization is found to be $\delta_{\text{nitr}} = 8 \pm 0.5\%$ and it does not depend on range. The value of δ_{nitr} reported in [12] is 9.8%; the discrepancy with our value may be related to different bandwidths of the receiving systems and as a result of different contributions of the nearest rotational Raman spectrum. The constant value of δ_{nitr} confirms that the geometrical factors are similar for both channels and these do not influence the ratio calculation for the altitudes above 400 m. The depolarization of the nitrogen Raman signal is the additional parameter that we use to control the correction factors in depolarization measurements. The depolarization ratio of water vapor at low altitudes, where the influence of the liquid-water Raman signal can be neglected, is about 14%. Liquid-water depolarization is much higher; it is 55% at 400 m and rises above 75% at 1200 m. As we have already mentioned, such a high value of δ_{liq} cannot be the result of bulk water depolarization, so it may be a result of the water-aerosol effect and the quick rise of δ_{liq} above 800 m probably reflects the changes in the aerosol parameters. The value of δ_{liq} significantly exceeds δ_{vap} ; hence bleed-through

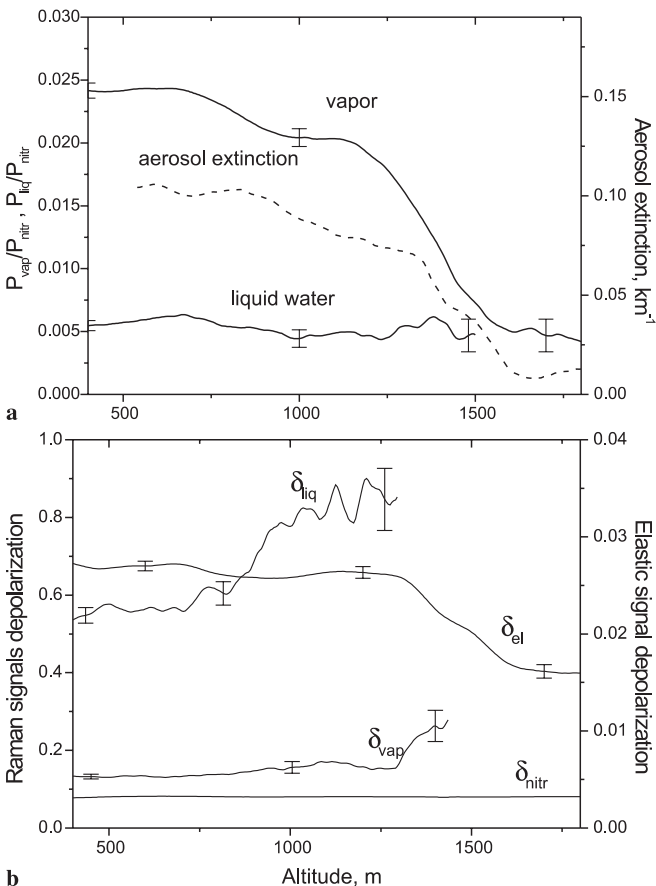


FIGURE 2 The ratios of liquid-water and water-vapor Raman signals to nitrogen Raman backscatter $P_{\text{liq}}/P_{\text{nitr}}$ and $P_{\text{vap}}/P_{\text{nitr}}$ (a) together with depolarization ratios of elastic δ_{el} and Raman signals from nitrogen δ_{nitr} , water vapor δ_{vap} and liquid water δ_{liq} (b) measured on 29 October 1999. The dashed line shows the aerosol-extinction profile evaluated by the Klett method for lidar ratio $B = 40$ sr⁻¹

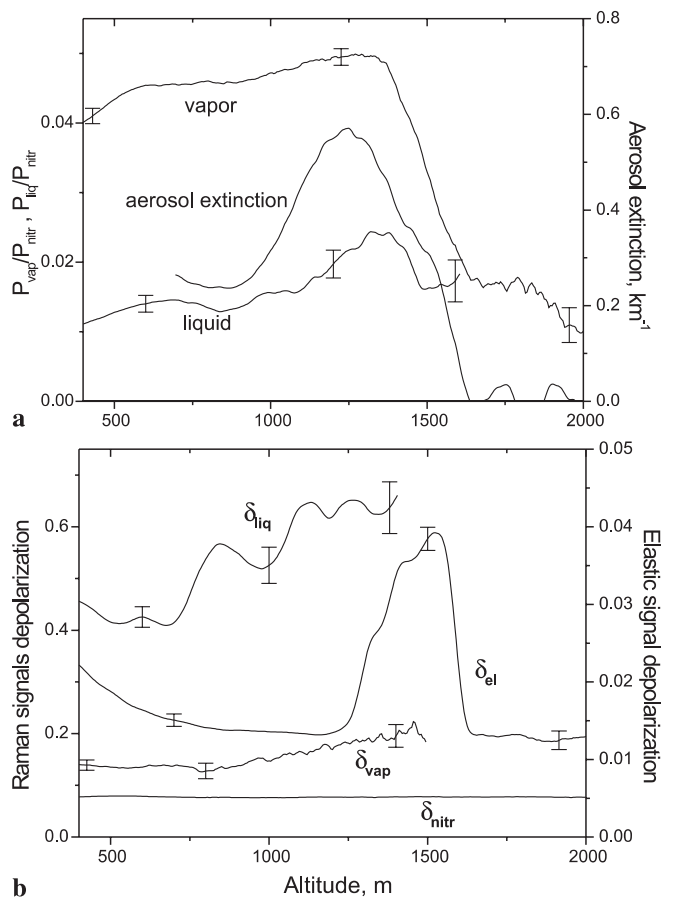


FIGURE 3 The ratios of liquid-water and water-vapor Raman signals to nitrogen Raman backscatter $P_{\text{liq}}/P_{\text{nitr}}$ and $P_{\text{vap}}/P_{\text{nitr}}$ (a) together with depolarization ratios of elastic δ_{el} and Raman signals from nitrogen δ_{nitr} , water vapor δ_{vap} and liquid water δ_{liq} (b) measured on 4 November 1999. The aerosol-extinction profile is evaluated by the Raman method

of liquid-water scattering should lead to the rise of water-vapor Raman-signal depolarization. This effect is observed above 1300 m, where the water-vapor content drops and the depolarization δ_{vap} rises to 20%. The depolarization of elastic backscatter is about 2.5% within the boundary layer and 1.5% above the PBL top. Such a behavior of δ_{el} indicates that the scattering is mainly due to the dry aerosols, which is consistent with low values of aerosol extinction and a low level of liquid-water Raman scattering.

The results observed on 4 November 1999 are shown in Fig. 3. Since the lidar ratio varies strongly near the PBL top, the extinction profile is calculated by the Raman method. For this day the ratio $P_{\text{liq}}/P_{\text{nitr}}$ at low altitudes is twice as high as it was on 29 October. The increase in aerosol extinction above 800 m coincides with $P_{\text{liq}}/P_{\text{nitr}}$ ratio growth and is associated with the rise of water-vapor Raman-signal depolarization. The depolarization of the elastic signal initially decreases, but above 1250 m abruptly rises to 4%. Such spikes in δ_{el} behavior near the PBL top were observed quite often, probably revealing that the layers consist of an irregularly shaped aerosol.

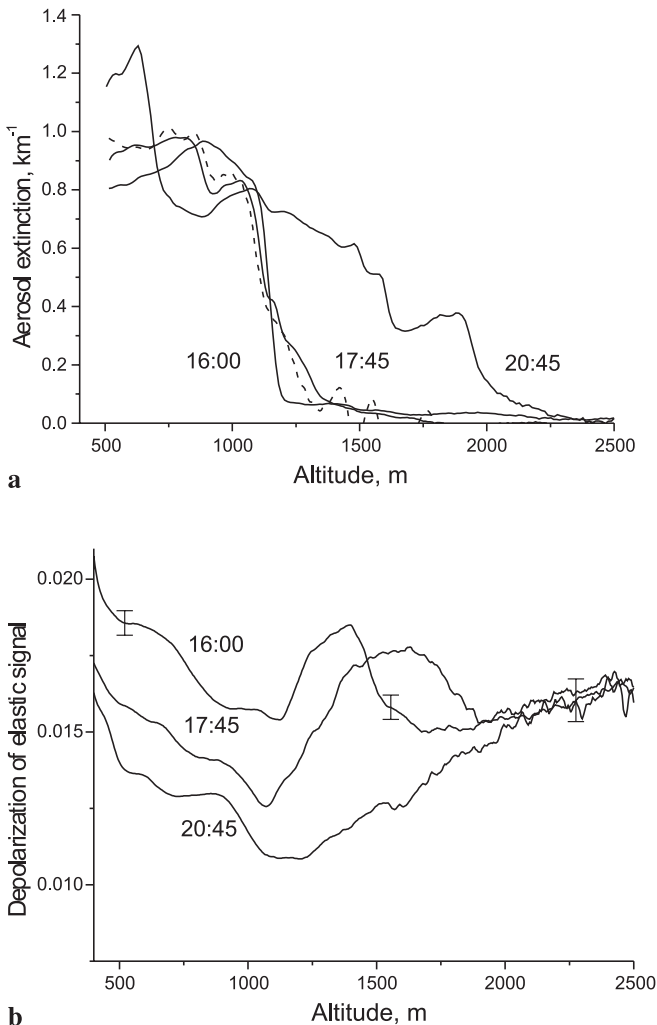


FIGURE 4 Aerosol-extinction profiles evaluated by the Klett method (a) and corresponding depolarization ratio of elastic signals (b) measured on 8 November 1999 during the 16:00–20:45 interval. The dashed line shows the extinction profile calculated by the Raman method

The results of temporal evolution of the PBL parameters on 8 November are presented in Fig. 4, which shows aerosol extinction and depolarization profiles obtained at 16:00, 17:45 and 20:45. The corresponding values of temperature at 27-m height are 17.3 °C, 15.8 °C and 13.2 °C and relative humidities are 53%, 59% and 75.5%. The extinction profiles are evaluated by the Klett method. One extinction profile, shown by a dashed line, was calculated by the Raman method. The lidar ratio on 8 November did not demonstrate large variations, so these methods give similar results. We use Klett inversion for illustration, because it allows us to calculate the extinction profiles for higher altitudes. The top of the PBL moves up with time and δ_{el} inside the PBL decreases. At 16:00, near the PBL top, the spike in δ_{el} behavior is distinctly visible, which indicates the presence of a dry aerosol. The upward PBL motion leads to the relative humidity rise at this altitude; the aerosol absorbs the moisture and transforms to spherical. As a result the spike becomes wider and then disappears completely. The temporal evolution of water-vapor and liquid-water profiles and the depolarization of Raman signals for the same day are shown in Figs. 5, 6. The liquid-water Raman scattering on 8 November was very high. As a result of the bleed-through effect, the value of δ_{vap} even at low altitudes is about 20% and increases with height up to $\sim 30\%$. The rise of water con-

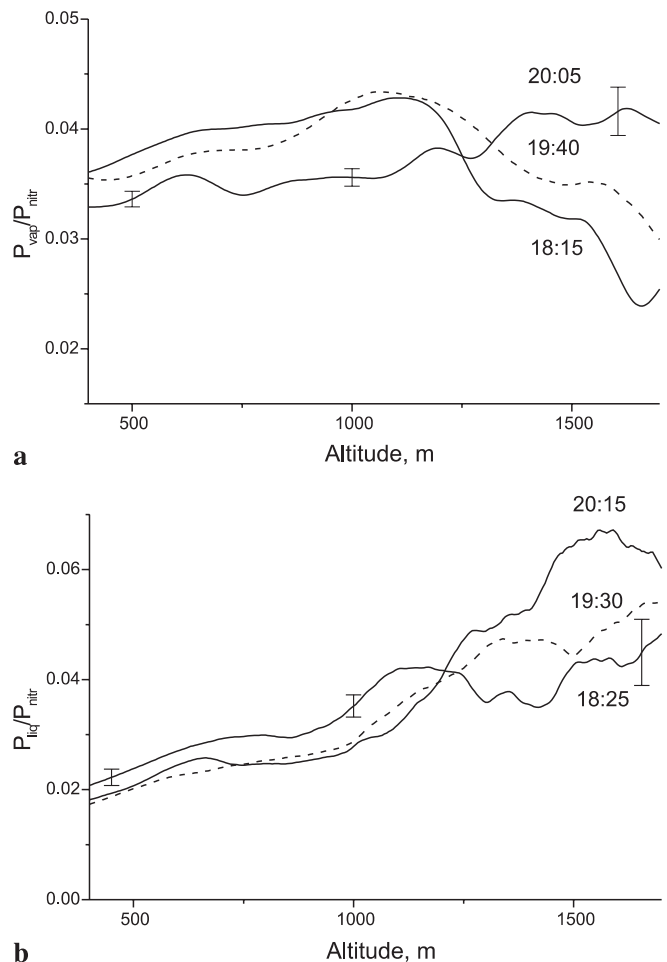


FIGURE 5 The ratios $P_{\text{vap}}/P_{\text{nitr}}$ (a) and $P_{\text{liq}}/P_{\text{nitr}}$ (b) measured on 8 November 1999

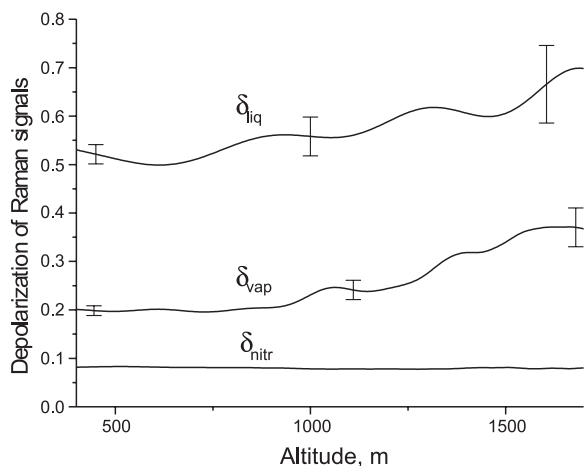


FIGURE 6 The depolarization ratios of Raman signals from nitrogen δ_{nitr} , water vapor δ_{vap} and liquid water δ_{liq} measured on 8 November 1999 around 20:00

tent in the PBL coincides with the decrease of elastic-signal depolarization.

A strong rise of the liquid-water signal may introduce significant errors in vapor measurements. To correct these errors knowledge of the exact water Raman contour is required.

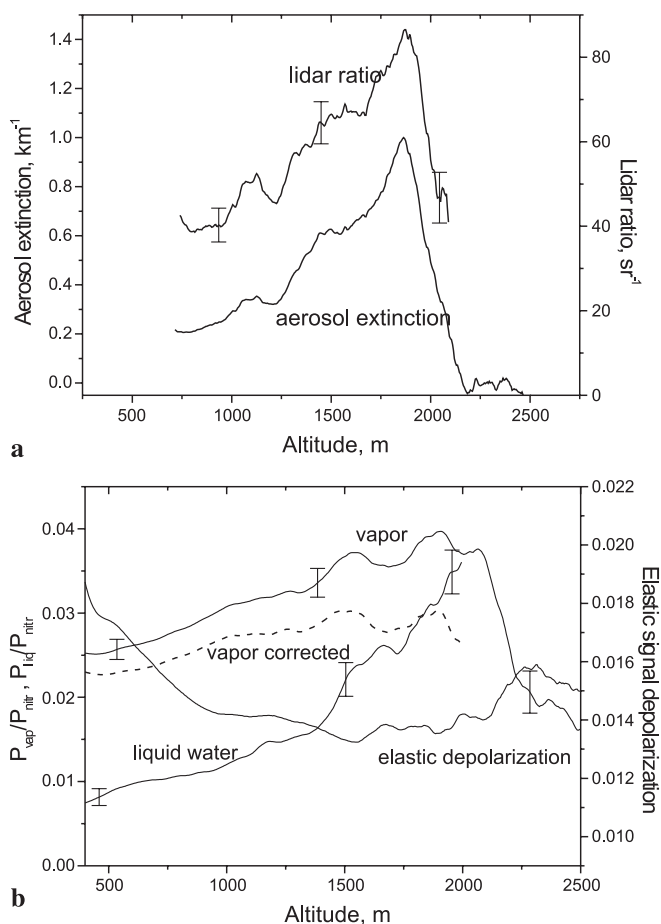


FIGURE 7 The lidar ratio and aerosol extinction calculated by the Raman method (a) together with $P_{\text{vap}}/P_{\text{nitr}}$ and $P_{\text{liq}}/P_{\text{nitr}}$ ratios and depolarization of elastic signals (b) measured on 9 November 1999. The dashed line in (b) shows the water-vapor profile corrected for the liquid-water interference

An attempt to correct the data obtained on 9 November is shown in Fig. 7. The aerosol-extinction profile obtained by the Raman method is shown together with the lidar ratio. The water Raman contour is calculated as a superposition of four Gaussian components; the average frequencies, half-widths of components and their percentages are taken from [18, 19]. The coefficients describing the cross-talk between liquid-water and water-vapor channels are calculated in the same manner, as was suggested in [7]. The water-vapor profile corrected for liquid-water influence is shown in Fig. 7b by the dashed line. After correction the content of water vapor near the PBL top is decreased by 20%. The liquid-water normalized Raman signal rises simultaneously with aerosol extinction, while the water-vapor signal does not change much. The liquid-water-content rise is accompanied by a decrease of elastic-signal depolarization. This example demonstrates the importance of liquid-water interference consideration, but unfortunately without independent radiosonde measurements we cannot verify how accurate such a correction is.

4 Conclusion

The separate detection of Raman signals performed in our experiment allows estimation of the relative intensities of Raman scattering by water-vapor and liquid-water aerosols inside the PBL for clear-sky conditions. The Raman scattering from atmospheric liquid water is surprisingly high. Its depolarization varies from 30% to 75%, and hence it cannot be the result of elastic-scattering bleed-through. If it was, the depolarization would be typical for elastic backscatter. The liquid-water scattering may introduce significant errors in water-vapor measurements, especially when wide-band excimer lasers are used for the sounding. Our results demonstrate that this interference may be controlled by measuring the depolarization ratio of the water-vapor Raman signal.

The final goal of our research is in obtaining quantitative information about the atmospheric water content from the Raman measurements. Such a technique will allow us to estimate water-droplet sizes [6] and lead to a better understanding of the process of cloud formation. To achieve this goal, further research attempts are required. Future directions of our activity in this field include the development of computer code for the calculation of Raman scattering by droplets, the measurement of the spectral shape of the liquid-water Raman backscatter from the atmosphere and the estimation of the contribution of water-vapor Raman rotational lines in the liquid-water Raman signal. These studies will help in accurate interpretation of experimental results and will lead to quantitative measurements of liquid water.

ACKNOWLEDGEMENTS The authors gratefully acknowledge Dr. D.N. Whiteman for supplying the experimentally measured water Raman contour.

REFERENCES

- 1 A. Ansmann, M. Riebesell, U. Wandinger, C. Weitkamp, E. Voss, W. Lahmann, W. Michaelis: *Appl. Phys. B* **55**, 18 (1992)
- 2 D.N. Whiteman, S.H. Melfi, R.A. Ferrare: *Appl. Opt.* **31**, 3068 (1992)
- 3 V. Sherlock, A. Garnier, A. Hauchecorne, P. Keckhut: *Appl. Opt.* **38**, 5838 (1999)

- 4 S.E. Bisson, J.E.M. Goldsmith, M.G. Mitchell: *Appl. Opt.* **38**, 1841 (1999)
- 5 S.H. Melfi, K.D. Evans, J. Li, D. Whiteman, R. Ferrare, G. Schwemmer: *Appl. Opt.* **36**, 3551 (1997)
- 6 D.N. Whiteman, S.H. Melfi: *J. Geophys. Res.* **D104**, 31 411 (1999)
- 7 I.A. Veselovskii, H.K. Cha, D.H. Kim, S.C. Choi, J.M. Lee: *Appl. Phys. B* **71**, 113 (2000)
- 8 M.I. Mishchenko, J.W. Honevier, L.D. Travis: *Light Scattering by Nonspherical Particles. Theory, Measurements, and Applications* (Academic, New York 2000)
- 9 T. Shibata, Y. Iwasaka, M. Fujiwara, M. Hayashi, M. Nagatani, K. Shiraishi, H. Adachi, T. Sakai, K. Susumu, Y. Nakura: *J. Geophys. Res.* **D102**, 10 829 (1997)
- 10 T. Sakai, T. Shibata, Y. Iwasaka: *J. Meteorol. Soc. Jpn.* **75**, 1179 (1997)
- 11 F. Cairo, G. Di Donfrancesco, A. Adriani, L. Pulvirenti, F. Fierli: *Appl. Opt.* **38**, 4425 (1999)
- 12 U. Wandering, A. Ansmann, C. Weitkamp: *Appl. Opt.* **33**, 5671 (1994)
- 13 M. Kerker, S.D. Druger: *Appl. Opt.* **18**, 1172 (1979)
- 14 D.N. Whiteman, G.E. Walrafen, W.-H. Yang, S.H. Melfi: *Appl. Opt.* **38**, 2614 (1999)
- 15 C.M. Penney, M. Lapp: *J. Opt. Soc. Am.* **66**, 422 (1976)
- 16 K. Cunningham, P.A. Lyons: *J. Chem. Phys.* **59**, 2132 (1973)
- 17 J.D. Klett: *Appl. Opt.* **24**, 1638 (1985)
- 18 J.R. Scherer, M.K. Go, S. Kint: *J. Phys. Chem.* **78**, 1304 (1974)
- 19 G.E. Walrafen: *J. Chem. Phys.* **47**, 114 (1967)